Free-energy calculations with multiple Gaussian modified ensembles

T. Neuhaus[1,*] and J. S. Hager[2,†]
[1]*NIC, Forschungszentrum Jülich, D-52425 Jülich, Germany*
[2]*Fachbereich Physik, Universität Duisburg-Essen, D-45117 Essen, Germany*
(Received 7 May 2006; published 12 September 2006)

We present a Monte Carlo algorithm, which samples free energies of complex systems. Less probable configurations are populated with the help of a multitude of additional Gaussian weights and parallel tempering is used for efficient Monte Carlo moves within phase space. The algorithm is easily parallelized and can be applied to a wide class of problems. We discuss algorithmic performance for the case of low-temperature phase separation in two-dimensional and three-dimensional Ising models, where we determine the magnetic interface tension. Multiple Gaussian modified ensemble simulations, unlike multicanonical ensemble simulations do not require *a priori* knowledge of the free energy and are of similar efficiency as multicanonical ensemble and Wang-Landau simulations.

DOI: 10.1103/PhysRevE.74.036702 PACS number(s): 02.70.−c, 05.50.+q

I. INTRODUCTION

In recent years, interest in complex systems has increased and one of the central computational challenges there is the determination of the free energy in theories with an underlying Gibbs measure. The properties of first-order phase transitions, glassy materials, proteins, and possibly many more complex systems all can be studied in terms of the free energy. In general, the partition function exhibits for certain parameter values several or even many distinct phase-space sectors separated by free-energy barriers corresponding to probable configurations. It is then a common feature of the class of problems considered here, that barrier-free energies are large at low temperatures or for systems with many degrees of freedom. Monte Carlo simulations are then confronted with a practical problem: Depending on the initial conditions, the Monte Carlo process can get stuck at a local maximum of the probability and full phase space is never sampled within reasonable amounts of computer time. It is thus of interest to develop efficient and robust Monte Carlo algorithms, like umbrella sampling [1] and multicanonical ensemble simulations [2,3], which address this and related sampling problems.

Several years ago, a solution to the particular exponential slowing-down problem at energy-driven first-order phase transitions was given [2,3]. In multicanonical ensemble simulations (muca) the rules of importance sampling are changed. At the transition point T_c of a first-order phase transition the suppression of configurations with mixed phases of droplets is lifted upon modifying the Boltzmann factor to

$$P_B = e^{-\beta_c E + W_{muca}(E)}, \tag{1.1}$$

with $\beta_c = 1/k_B T_c$ the inverse transition temperature and $\exp[W_{muca}(E)]$ denoting the multicanonical weight factor. The logarithmic weight is chosen to approximate

$$W_{muca}(E) \approx -\ln g(E) + \beta_c E + \text{const}, \tag{1.2}$$

where $g(E)$ denotes the number density of states at energy E. In particular, we find the multicanonical partition function

$$Z_{muca} \approx \text{const} \sum_{\text{conf}} g^{-1}(E) \tag{1.3}$$

and thus the Monte Carlo process visits all configurations at energies E, even for energies within the mixed phase, with almost equal probability $P_{muca}(E) \approx \text{const}$. In multicanonical ensemble simulations it is possible to choose a polygon for the curve $W_{muca}(E)$ with a piecewise representation

$$W_{muca}(E) = -\Delta\beta_i E + c_i \tag{1.4}$$

on some carefully selected energy intervals $E_i \leqslant E < E_{i+1}$ with $i = 1, \ldots, N_{muca}$. The Boltzmann factor of Eq. (1.1) has almost the canonical form $P_B = \exp[-\hat{\beta}_i E + c_i]$ with an energy-dependent inverse temperature $\hat{\beta}_i = \beta_c + \Delta\beta_i$ and the latter property determined the name, multicanonical ensemble. The canonical probability distributions $P_{\text{can}}(E)$ of the energy are recovered with a final reweighting step

$$P_{\text{can}}(E) \propto e^{-W_{muca}(E)} P_{muca}(E) \tag{1.5}$$

quite analog to the reweighting introduced a long time ago by the pioneering work of Ferrenberg and Swendsen [4].

Multicanonical ensemble simulations at first-order phase transitions are designed to reduce exponentially large ergodicity Monte Carlo time scales

$$\tau_E \propto e^{+F_B} \tag{1.6}$$

caused by barrier-free energies F_B, which for first-order phase transitions of d-dimensional systems on L^d boxes typically behave as

$$F_B = \text{const}\, L^{d-1}, \tag{1.7}$$

with a value of const $\approx 2\sigma_0$.[1] Exponential slowing down in multicanonical ensemble simulations is reduced significantly,

*Email address: t.neuhaus@fz-juelich.de
†Email address: johannes@theo-phy.uni-essen.de

[1]Barrier spin configurations on two-dimensional (2D) L^2 boxes contain a lens-shaped droplet with $F_B = 2.2692\ldots\hat{\sigma}L$.

though cannot be avoided completely. For two-dimensional (2D) systems it was shown in a recent work [5] that crystal-shape phase transitions within the two-phase separated phase-space region and the evaporation/condensation (E/C) phase transition from a gas of small droplets to a large nucleated droplet cause additional free-energy barriers

$$F_{B,\mathrm{crystal}} = 0.1346 \ldots 2\hat{\sigma}L, \tag{1.8}$$

$$F_{B,E/C} = cL^{2/3}, \tag{1.9}$$

with $\hat{\sigma}$ denoting the effective interface tension from the Wulff construction for droplets and a value of c as given in Ref. [5]. The maximum value

$$F_{B,\mathrm{crystal}} = \max[F_{B,\mathrm{crystal}}, F_{B,E/C}] \tag{1.10}$$

determines the rate of residual exponential slowing down in multicanonical ensemble simulations of 2D systems for large system sizes. A generalization of this result to higher-dimensional systems is nontrivial and did not yet appear in the literature. Nevertheless, production type multicanonical ensemble simulations of first-order phase transitions in spin models, as well as in lattice gauge theories, have demonstrated large efficiency gains if algorithmic performance is compared to standard Monte Carlo methods. The idea of Boltzmann-factor modification towards flat histogram sampling has also been generalized to other thermodynamic observables, e.g., order parameters. Multicanonical ensemble simulations have been successfully applied to spin glasses by sampling flat Parisi overlap order-parameter distributions, and to the simulation of protein models, polymers and chains. Some of the recent progress in the simulation of these theories relies on the efficiency of multicanonical ensemble simulations. For a recent review we refer to Ref. [6].

Multicanonical ensemble simulations have, however, a practical disadvantage. They require an estimate on the density-of-states function, which determines the multicanonical weight. In practice it turned out that there are many ways to find approximations to the density of states, but the situation remains somewhat unsystematic; depending on the problem under study, different strategies were used. These include finite-size scaling—or the recursive construction of weights—or density-of-states sampling on energy patches. Recently, Wang and Landau [7,8] reported on an efficient non-Gibbsian Monte Carlo method for the direct sampling of the density-of-states function, which can also be used as an input to multicanonical ensemble simulations.

Any Monte Carlo algorithm designed for the efficient exploration of the free-energy landscape must visit all relevant configurations with a large enough probability, those which are probable and those on the barrier. Years ago, Challa and Hetherington [9–11] introduced the Gaussian ensemble as an interpolation between the microcanonical and the canonical ensemble in studies of the phase transition in the q-state Potts model. Later, Challa and Landau studied the issue for the case of first-order phase transitions [12]. Their observation was, that in modified ensembles, where the Boltzmann factor is multiplied by an exponential of a negative quadratic form, i.e., a Gaussian

$$Z_{GME}(E_0, \Delta E_0) = \sum_{\mathrm{conf}} e^{-\beta_c E - [(E - E_0)^2/\Delta E_0^2]}, \tag{1.11}$$

configurations with energy E can be sampled, centered with large probability close to any value E_0, if only the parameter ΔE_0 is chosen to be small enough. This single *Gaussian modified ensemble* (GME) was simulated with standard Monte Carlo methods for values of E_0 within the mixed phase of a first-order phase transition and some information on the first-order phase transition properties was extracted. However, using this idea never became popular in realistic studies as it was not established to what degree of efficiency the algorithm was able to move all the relevant excitations within the mixed phase. Similar ideas were also presented by Bhanot *et al.* in a sequence of papers [13], where the Gaussian of Eq. (1.11) was replaced by a step function of finite width and infinite height. They were interested in a Monte Carlo sampling method for the energy density of states and the calculation of partition-function zeros. Recently, Virnau and Müller [14] proposed an implementation of the above ideas through successive umbrella sampling and tested it in grand canonical simulations of a Lennard-Jones fluid. In this paper we introduce the *multiple Gaussian modified ensemble* (MGME), which takes the product form

$$Z_{MGME}(E_1, \ldots, E_N; \Delta E_1, \ldots, \Delta E_N) = \prod_{i=1}^{N} Z_{GME}(E_i, \Delta E_i) \tag{1.12}$$

of a multitude of single Gaussian modified ensembles $i = 1, \ldots, N$. We show, that all relevant configurations within the free-energy landscape can be populated for suitable values of E_i and ΔE_i, and how the density of states $g(E)$ can be determined from a Monte Carlo simulation of Z_{MGME}. There exists also an efficient Monte Carlo update to sample Z_{MGME}, which is parallel tempering.

Parallel tempering [15–18] originally was introduced to reduce large autocorrelation times in spin-glass simulations. A similar product form to the one of Eq. (1.12),

$$Z_{\mathrm{glass}}(T_1, \ldots, T_N) = \prod_{i=1}^{N} Z_{\mathrm{glass}}(T_i), \tag{1.13}$$

with N different glassy canonical partition functions $Z_{\mathrm{glass}}(T_i)$, is updated with parallel tempering moves. The similarity of Z_{glass} with Z_{MGME} suggests that parallel tempering can also be used efficiently in MGME simulations.

In this paper we combine MGME simulations with parallel tempering for the sampling of barrier-suppressed states. MGME simulations eliminate the necessity to generate multicanonical weights in the first place, at the price of larger computer memory requirements. At the same time, the advantages of flat—or almost flat—histogram sampling are kept. We organize the paper as follows: Sec. II introduces the MGME. Several subsections describe in detail issues like the measurement of canonical probabilities, the choice of Gaussian weights, and aspects of parallel tempering. Section III reviews theoretical results for our test systems, which are the 2D and 3D Ising models. Section IV compares the perfor-

mance of MGME simulations for the barrier calculation with multicanonical ensemble and Wang-Landau simulations. Section V concludes the paper.

II. MULTIPLE GAUSSIAN MODIFIED ENSEMBLES

The partition function of the MGME is defined to be

$$Z_{MGME}(A_1,\ldots,A_N;\Delta A_1,\ldots,\Delta A_N)=\prod_{i=1}^{N} Z_{GME}(A_i,\Delta A_i), \tag{2.1}$$

where $Z_{GME}(A_i,\Delta A_i)$ with $i=1,\ldots,N$,

$$Z_{GME}(A_i,\Delta A_i)=\sum_{\text{conf}} e^{-\beta E-[(A-A_i)^2/\Delta A_i^2]} \tag{2.2}$$

is a single Gaussian modified partition function. We consider statistical mechanics models in arbitrary dimension d as specified by their Hamiltonian H at inverse temperature $\beta=1/k_BT$. In a generalization of the original Challa and Landau idea, we work with any thermodynamic observable A of physical interest. It can be the energy $A=E$, or in magnetic systems the magnetization $A=M$, or for the spin-glass case, the Parisi overlap order parameter $A=Q$. In general, A is extensive and MGME simulations yield a stochastic approximant to the probability distribution function $P(A)$,

$$P(A)=\frac{1}{Z}\sum_{\text{conf}} \delta(A-A_{\text{conf}})e^{-\beta H} \tag{2.3}$$

for the occurrence of a specific A value with normalized probability $P(A)$ in the canonical ensemble Z of the theory.

The probability distribution function $P(A)$ contains the desired physical information on the free-energy landscape of the theory. The function $P(A)$ has possibly several stable extremal points at observable values $A_{\max}$ for probable configurations and possibly several unstable ones at values $A_{\min}$ for free-energy suppressed configurations. Free-energy barriers

$$F_B=\ln\frac{P(A_{\max})}{P(A_{\min})} \tag{2.4}$$

can have large values and may diverge with some power of the linear system size L. In particular, we may choose A to be the magnetization M for magnetic theories with $Z(2)$ symmetry like the Ising model, in which case the magnetization probability distribution function $P(M)$ develops double peaks at low temperature and

$$\sigma_B(L)=\frac{1}{2}\frac{F_B}{L^{d-1}} \tag{2.5}$$

turns into Binder's definition of the magnetic interface tension, with

$$\lim_{L\to\infty}\sigma_{\text{Binder}}(L)=\sigma_0. \tag{2.6}$$

Interface-free energies can be calculated with Binder's method, but in addition there exist other and in certain cases more efficient methods, like the calculation of σ from tunneling masses on elongated boxes [19,20], or the integration of surface free-energy densities along temperature directions [21].

We may also choose $A=E$. The probability distribution function $P(E)$ of the energy

$$\ln g(E)=\ln P(E)+\beta E+\text{const}, \tag{2.7}$$

then is related to the number density of states $g(E)$ up to an unknown factor and MGME simulations turn into a density-of-states sampling method. At $\beta=\beta_c$ and for energy-driven first-order phase transitions $P(E)$ again develops double peaks. The interface tension in-between ordered and disordered bulk states can be determined in a similar way as for the magnetic case Eq. (2.6).

The Monte Carlo evaluation of the MGME determines the probability distribution function $P_{MGME}(A)$ for the occurrence of a specific A value within Z_{MGME}. Then one employs known properties and derives the canonical probability $P(A)$ from the measured $P_{MGME}(A)$ data.

A. Probability measurements

The probability distribution function $P_{MGME}(A)$ is obtained by inserting the sum over the Kronecker symbol $\delta(A-A_{\text{conf},i})$,

$$Z_{MGME}^{-1}\sum_{i=1}^{N}\delta(A-A_{\text{conf},i}) \tag{2.8}$$

into the MGME partition function Z_{MGME}. A stochastic approximant to this probability is obtained numerically upon forming a histogram from all configurational values A within the Monte Carlo simulation [see Eq. (2.25)]. Formally, this equals the sum

$$P_{MGME}(A)=\frac{1}{N}\sum_{i=1}^{N}P_{GME,i}(A), \tag{2.9}$$

where the latter $P_{GME,i}(A)$ denotes normalized probabilities for finding values A in single GME partition functions $Z_{GME,i}$;

$$P_{GME,i}(A)=Z_{GME,i}^{-1}\sum_{\text{conf}}\delta(A-A_{\text{conf},i})e^{-\beta H-[(A-A_i)^2/\Delta A_i^2]}, \tag{2.10}$$

which finally are related to the canonical probability $P(A)$ of Eq. (2.3) via a reweighting step

$$P_{GME,i}(A)=P(A)e^{-F_i-[(A-A_i)^2/\Delta A_i^2]}, \tag{2.11}$$

where the "free-energy constants" F_i guarantee correct normalizations. We observe that Eqs. (2.9) and (2.11) imply the equations

$$\ln P(A)=\ln P_{MGME}(A)+\ln N-\ln\left\{\sum_{i=1}^{N}e^{-F_i-[(A-A_i)^2/\Delta A_i^2]}\right\}, \tag{2.12}$$

$$F_i = \ln\left\{ \sum_A P(A) e^{-[(A-A_i)^2/\Delta A_i^2]} \right\}, \quad i = 1, \ldots, N, \tag{2.13}$$

which for a given input $P_{MGME}(A)$ constitute an equation system for $i=1,\ldots,N$ unknown values of F_i and the normalized $P(A)$. A similar, but nonidentical equation system, has surfaced some time ago in the context of Ferrenberg Swendsen multihistogram reweighting techniques [4] and there it was shown that a unique solution exists. The solution can be constructed to arbitrary precision with the help of a recursive iteration, which for the purposes of the present paper was simply adopted to the solution of the current problem. In this way the measured probability $P_{MGME}(A)$ determines a stochastic approximation to the canonical probability $P(A)$.

B. Populating phase space

MGME simulations populate configurations, for which the values of the thermodynamic observable A lie within some extensive interval of size L^d. The probability distribution function $P_{MGME}(A)$ of Eq. (2.9) is expected to have finite, i.e., larger than exponentially small values on the interval

$$A_- \leqslant A \leqslant A_+, \tag{2.14}$$

with an interval length $A_+ - A_- \propto V$ growing linear with the volume $V=L^d$. By construction one obtains the probability distribution function $P_{MGME}(A)$ through the superposition of N single GME probability distribution functions, Eqs. (2.9) and (2.10), whose maximum peak probability values ought to be centered at specified points and, whose individual width ought to be broad enough to accommodate all A values between the maximum positions of neighboring distributions. In an attempt to fulfill these requirements we introduce the MGME1 version of our sampling method and consider an equal partition

$$A_i = A_- + (i-1)\frac{A_+ - A_-}{N-1}, \quad i = 1, \ldots, N \tag{2.15}$$

of the interval $[A_-, A_+]$, fixing the Gaussian central positions of the partition function $Z_{MGME}(A_1, \ldots, A_N; \Delta A_1, \ldots, \Delta A_N)$ accordingly. In addition, the width of the Gaussians is chosen to be constant,

$$\Delta A_i = \Delta A = \frac{A_+ - A_-}{N-1}, \quad i = 1, \ldots, N. \tag{2.16}$$

It is quite clear, that depending on the problem under study, the number N eventually has to be tuned to large values if large barriers F_B are studied. A limiting case appears to be the case of a regular free-energy landscape with finite derivatives $\partial_A \ln P(A)$ in the thermodynamic limit. In this case one can populate all A values with nonexponentially small probabilities if N only is tuned $N \propto \sqrt{V}$. This behavior presumably constitutes a lower bound for the number N necessary in all realistic studies of barrier-free energies with MGME simulations. In this work we scale

$$N \propto L^{d-1} \tag{2.17}$$

and thus the ratio N/F_B is fixed at a constant value. In a second and more elaborate scheme, denoted the MGME2 version here, we relate the Gaussian width via

$$\Delta A_i = \Delta A = \text{const}\,\frac{A_+ - A_-}{F_B}, \quad i = 1, \ldots, N \tag{2.18}$$

to the barrier height and fix the Gaussian central positions through a constant overlap criterion

$$O_{i,i+1} = \sum_A \min[P_{GME,i}(A), P_{GME,i+1}(A)] \approx 0.63, \quad i = 1, \ldots, N-1, \tag{2.19}$$

on neighboring $i, i+1$ Gaussian modified distributions, where the single Gaussian probabilities are normalized to unity $1 = \Sigma_A P_{GME,i}(A)$. This particular overlap formula, and the specific choice of the constant 0.63, ensure Metropolis acceptance rates $P_{\text{acc}} \approx 0.5$ in the latter parallel tempering swaps of neighboring GMEs. MGME2 simulations utilize a nonequidistant spacing of the Gaussian central positions, but again the ratio N/F_B is constant for large boxes. We will find that values N/F_B of order unity can be used to populate the phase space.

C. Monte Carlo simulation and parallel tempering

The partition function of the MGME Eq. (2.1) is evaluated with the help of Monte Carlo sampling methods in the standard way. One generates a Markov chain of configurations with transition probabilities that respect detailed balance. It is somewhat less standard that the configuration space of MGME simulations contains N different spin configurations at any step on the Markov chain. We imagine these spin configurations to be stored on N different nodes of a parallel computer, where each node carries a node number $\alpha = 1, \ldots, N$. There are also $i=1,\ldots,N$ different single GMEs as labeled by their ensemble indices i, which are uniquely mapped to nodes or actual spin configurations. Let us denote the map from ensemble indices to nodes $\alpha(i)$ and the inverse $i(\alpha)$. Both, the spin configurations on the nodes and the assignment of nodes to single GMEs are updated during the Markov process. This way it can happen that spin configurations on the $\alpha=1$ node for some steps on the Markov process represent spin configurations of the $i=1$ single GME, while in later steps another, possibly the $i=N$ ensemble, is updated on the same node.

Clearly the first thing to do are local Monte Carlo updates of spin degrees of freedom. One sweep is defined to be the consecutive local update of all spins. This makes a total of $N \times V$ Monte Carlo steps per sweep,

$$1\ \text{Sweep} = N \times V\ \text{Monte Carlo steps}. \tag{2.20}$$

In the present paper local heatbath updates for Ising spins are used. The spin Hamiltonian depends on the node number and the map $i(\alpha)$ for any spin. Different ensemble indices i require updates within different single GMEs.

In parallel tempering one employs the MGME property that any two probability distributions $P_{GME,i}(A)$ and

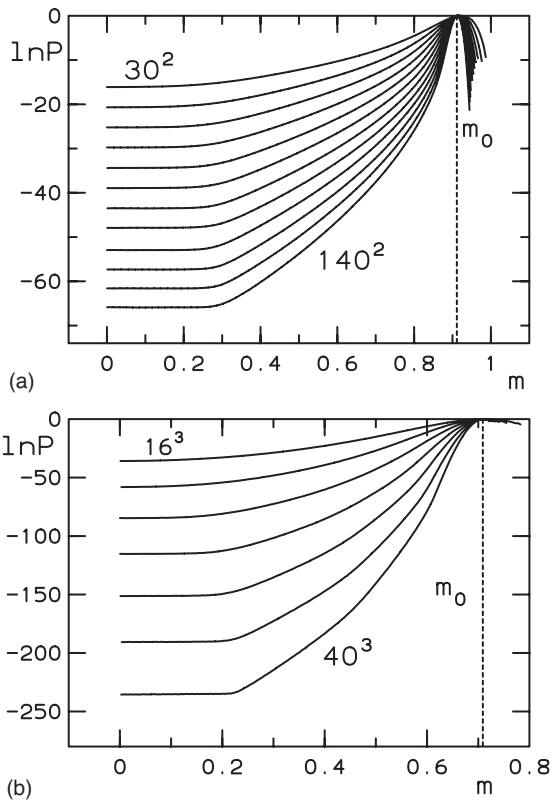

FIG. 1. Logarithmic probability distribution function $P(m)$ of Eq. (3.3) from MGME2 simulations as a function of the magnetization density $m=M/V$. The top panel shows 2D data at $\beta=0.5$ with lattice sizes L ranging from $L=30$ to $L=140$ in steps of unit 10. The bottom panel shows 3D data at $\beta=0.2439$ with lattice sizes L ranging from $L=16$ to $L=40$ in steps of unit 4. The dashed vertical lines denote the infinite volume-magnetization values at m_0.

$P_{GME,j}(A)$ of single GMEs have a finite overlap [see Eq. (2.19)] for MGME2 simulations if their ensemble indices i and j correspond to nearest neighbors $|i-j|=1$ in the partition of Eq. (2.15). Let us denote by $A(\alpha,n_s)$ the value of the thermodynamic observable on the node α at the sweep n_s, while the total number of sweeps is denoted N_s. In particular, we expect that nearby A values with

$$|A(\alpha(i),n_s)-A(\alpha(j),n_s)|\approx\Delta A \tag{2.21}$$

can easily be found with finite probability in the Markov chain. The parallel tempering (pt) move

$$\alpha(i)\{n_s+\text{one pt move}\}=\alpha(j)\{n_s\},$$

$$\alpha(j)\{n_s+\text{one pt move}\}=\alpha(i)\{n_s\}, \tag{2.22}$$

is governed by the Metropolis acceptance rate

$$P_{\text{acc}}=\min[1,e^{-\Delta G}] \tag{2.23}$$

with

$$\Delta G=-\frac{[A(\alpha(j),n_s)-A_i]^2+[A(\alpha(i),n_s)-A_j]^2}{\Delta A^2}+\frac{[A(\alpha(i),n_s)-A_i]^2+[A(\alpha(j),n_s)-A_j]^2}{\Delta A^2} \tag{2.24}$$

and results into updates with finite acceptances, $P_{\text{acc}}\approx 0.5$ for MGME2 simulations. Technically and in the context of the present paper, each sweep with local updates is supplemented by exactly N parallel tempering moves on pairs of neighboring i and j values, which are randomly drawn from the set of all neighboring pairs. Parallel tempering only uses a small fraction of the amount of computer time spent in local spin updates.

Finally, we arrive at a stochastic approximant

$$P_{MGME}(A)=\frac{1}{N}\sum_{\alpha=1}^{N}\frac{1}{N_s}\sum_{n_s=1}^{N_S}\delta[A-A(\alpha,n_s)] \tag{2.25}$$

to the probability distribution function $P_{MGME}(A)$ of Eq. (2.9), which as described in Sec. II A, is used to measure the canonical probability $P(A)$.

III. KNOWN RESULTS FOR 2D AND 3D ISING MODELS

The present study uses the two- and the three-dimensional ferromagnetic Ising models in their $Z(2)$ symmetry-broken phase at low temperature to investigate the efficiency of MGME simulations for the calculation of barrier-free energies. The 2D Ising model is conceptually simple and it allows us to use rigorous results in the comparison to high-precision simulation data, which are obtained from our new simulation technique. The partition function of the Ising model is given by

$$Z=\sum_{\text{conf}}e^{-\beta H}, \tag{3.1}$$

with the zero-field Hamiltonian

$$H:=-\sum_{\langle i,j\rangle}s_i s_j, \tag{3.2}$$

where H contains the usual nearest-neighbor interaction of spins $s_i=\pm 1$. Our efforts will be focused on the probability distribution function

$$P(M)=\frac{1}{Z}\sum_{\text{conf}}\delta\left(M-\sum_i s_i\right)e^{-\beta H}, \tag{3.3}$$

which is proportional to the constraint-magnetization partition function $P(M)\propto Z(m,\beta)$. The thermodynamic observable A here corresponds to the magnetization M and $m=M/V$ is the magnetization density. In 2D we study the theory at $\beta=0.5$, i.e., for temperatures $T/T_c=0.88\ldots$ below the critical point $\beta_c=\ln(1+\sqrt{2})/2$. In 3D we choose $\beta=0.2439$ at $T/T_c=0.59\ldots$ with $\beta_c\approx 0.41$. In the low-temperature phase the probability distribution function $P(M)$ develops double peaks and most probable configurations are located at magnetization densities $m=\pm m_{\max}$. For given parameters and on large boxes $m_{\max}$ will approach Onsager's

TABLE I. Run parameters for MGME2 Ising-model simulations in 2D (β=0.5) and 3D (β=0.2439). L denotes the box size while N is the number of GMEs. M_- and M_+ denote the (extensive) observable interval and ΔM is the Gaussian width, which with increasing size increases linearly in L. The number N has a constant value in units of the barrier F_B.

D	L	N	M_-	M_+	ΔM	N/F_B
2	30	10	−27	888	131.39	0.73
2	40	16	−62	1562	149.96	0.88
2	50	22	−18	2418	166.18	0.96
2	60	28	−8	3462	186.85	1.02
2	70	34	−109	4694	213.14	1.06
2	80	40	−152	6110	236.73	1.10
2	90	44	−130	7716	269.75	1.07
2	100	50	−189	9496	293.34	1.10
2	110	55	−120	11474	319.59	1.10
2	120	59	−21	13638	351.03	1.08
2	130	64	−226	15980	383.56	1.08
2	140	68	−124	18514	414.82	1.06
3	16	13	−23	2924	326.04	0.34
3	20	22	−186	5692	391.68	0.37
3	24	32	−289	9800	462.42	0.38
3	28	43	−245	15582	538.87	0.37
3	32	56	−210	23312	613.91	0.37
3	36	71	−341	33112	688.48	0.37
3	40	85	−125	45454	782.32	0.36

magnetization value $m_0=0.911\,319\ldots$ in 2D, while $m_0=0.709\,13(7)$ was measured in 3D [22]. The 2D planar interface tension $\sigma_0=2+\ln[\tanh(\beta)]/\beta$ in-between bulk phases of opposite magnetization at $\beta=0.5$ has the exact value $\sigma_0=0.228\,063\ldots$ [23], while in 3D at $\beta=0.2439$, $\sigma_0=0.074\,03(30)$ was determined in numerical simulations [22]. Interface tensions determine the asymptotic large L behavior of the barrier-free energy

$$F_B=\ln\frac{P(m_{\max})}{P(m=0)}\propto 2\sigma_0 L^{d-1} \tag{3.4}$$

for boxes of size $V=L^d$ with periodic boundary conditions. For purposes of orientation, we display in Fig. 1 our final results for the probability distribution functions $P(M)$ for the 2D (top panel) and the 3D (bottom panel) cases. We display results from MGME2 simulations on lattices with volumes 30^2 to 140^2 in 2D and volumes 16^3 to 40^3 in 3D. It can be noted that the largest barrier values are about $F_B\approx 65$ in 2D and $F_B\approx 235$ in 3D.

2D distributions $P(M)$ were already studied in Ref. [24] with the aim to understand the dynamics of the decay of metastable states. A particular interesting aspect, which recently received some interest, is the existence of an evaporation-condensation (E/C) phase transition [25] within the Ising models $Z(m,\beta)$ [26,5,27,28].

IV. RESULTS OF SIMULATIONS

MGME simulations are implemented for the 2D and 3D Ising models along the lines of the previous sections. In 2D and at $\beta=0.5$ it was decided to simulate L^2 boxes with periodic boundary conditions on lattice sizes L ranging from $L=30$ up to $L=140$. In 3D at $\beta=0.2439$ we simulated L^3 boxes with periodic boundary conditions on lattice sizes L ranging from $L=16$ up to $L=40$. In 2D as well as in 3D we first conducted a set of MGME1 simulations with an observable interval

$$A_-=M_-=0,\quad A_+=M_+=V. \tag{4.1}$$

The corresponding number N of GME tunings had the L dependencies $N(L)=(L/2)+1$ for 2D and $N(L)=(L+1)^2/41$ in 3D. In a second round of MGME2 simulations we tuned the Gaussian width as

$$\Delta M=1\frac{m_0V}{F_B(L)} \tag{4.2}$$

in 2D and as

$$\Delta M=4\frac{m_0V}{F_B(L)} \tag{4.3}$$

in 3D. The MGME1 estimate for the canonical probability $P(M)$ then determines $P_{GME,i}(M)$, which satisfies the constant overlap criterion of Eq. (2.19), fixing the Gaussian central positions. In 2D the total number of sweeps N_s [see Eq. (2.20)] was $N_s=10^6[(L/2)+1]/N$ for each single Monte Carlo run MGME1 or MGME2 at given L. On our largest system with $L=140$ the total statistics accumulates to 1.4×10^{12} single-spin heat bath steps and to 7.1×10^7 parallel

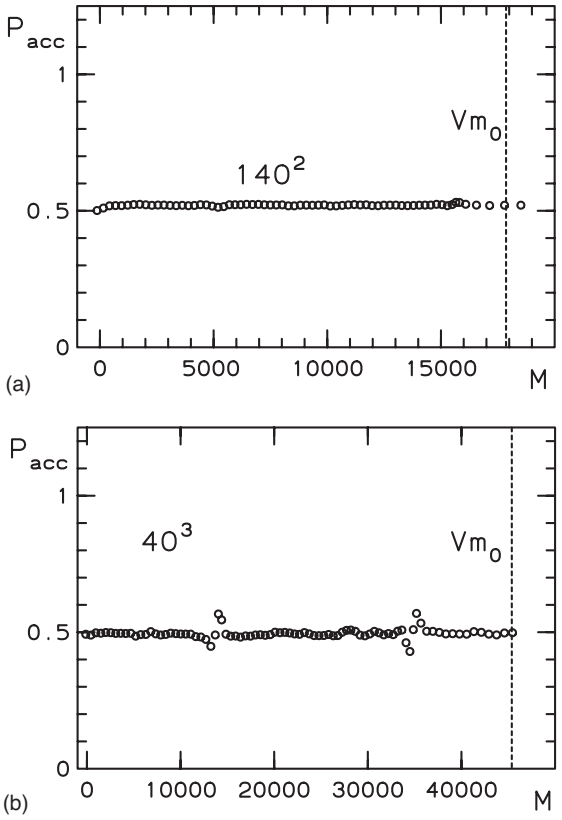

FIG. 2. Acceptance rates $\langle P_{\mathrm{acc}} \rangle$ of parallel tempering swaps in MGME2 simulations as a function of the Gaussian central positions M_i, $i=1,\ldots,N$ with $N=68$ on a 2D 140^2 box on the top and with $N=85$ on a 3D 40^3 box on the bottom.

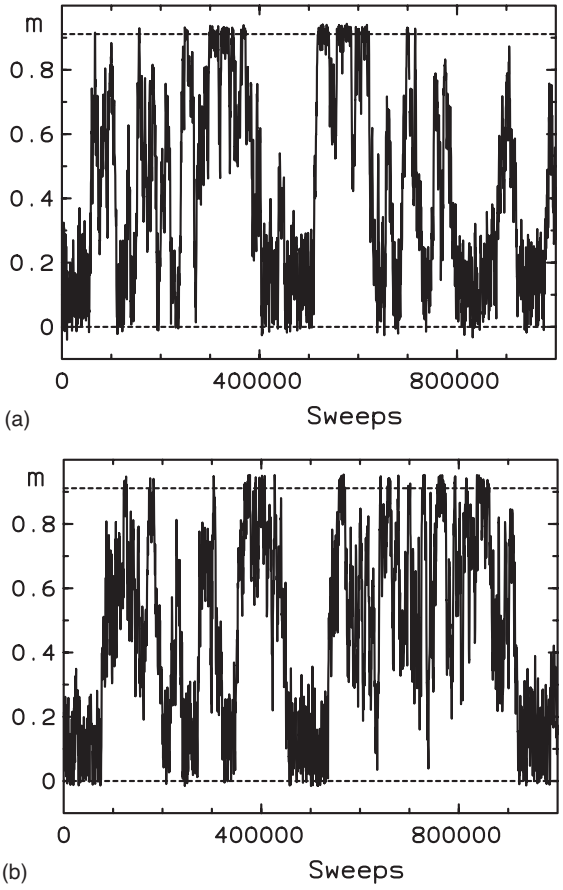

FIG. 3. (a) Magnetization density m time series in the 2D Ising model for MGME simulations (MGME1) on a 80^2 lattice with a number of GMEs $N=41$. The time series has a length of 10^6 sweeps and is obtained from configurations, which reside on the first node. Similar time series exist on an additional 40 nodes, which, however, cannot be displayed. (b) Magnetization density m Monte Carlo time series for multicanonical ensemble simulations on a 80^2 lattice at the same parameters. We display a series of 10^6 sweeps from a total run having a length of 41×10^6 sweeps. The lower dashed lines in both panels are at $m=0$, while the upper ones have $m=m_0$.

tempering updates. In 3D the total number of sweeps N_s [see Eq. (2.20)] was kept at a rather small number $N_s=4\times10^6/N$ in order to facilitate a one-to-one comparison to the data in Ref. [22], which have 4×10^6 sweeps in multicanonical simulations. Some run parameters, like the number N of Gaussians as a function of the system size L can be found in Table I.

The Metropolis acceptance rates of MGME2 parallel tempering updates turned out to be close to $\langle P_{\mathrm{acc}} \rangle \approx 0.5$ in the mean, for all of our runs. The dependencies of $\langle P_{\mathrm{acc}} \rangle$ on the Gaussian central positions M_i with $i=1,\ldots,N$ are displayed in Fig. 2 on the 2D 140^2 box (top panel) and the 3D 40^3 box (bottom panel).

Parallel tempering moves are designed to ensure ergodicity and configuration transport to arbitrary phase-space locations. The use of parallel tempering in a 2D MGME simulation can be witnessed in the top panel of Fig. 3, where a MGME1 magnetization density time series is displayed for a particular node out of 41 nodes on the 80^2 lattice. The Monte Carlo process visits configurations at $m\approx0$, the lower dashed horizontal line, as well as densities at $m\approx m_0$, the upper dashed horizontal line, and a typical ergodicity time scale appears to be several ten thousand sweeps for the given lattice size. The bottom panel shows a time series from flat-histogram multicanonical simulations at the same values of parameters. Judging by the eye, both simulations perform at a similar level of efficiency. Unfortunately, MGME1 as well as MGME2 simulations, only support autocorrelation-time measurement intervals, which are smaller by a factor N^{-1}, as compared to, e.g., multicanonical simulations at the same number of local spin updates. We therefore do not study ergodicity time scales here in great detail. Instead we judge the efficiency of our various simulational approaches by the magnitude of the statistical error on Binder's interface tension value σ_B. All of our analysis is based on jackknife-method statistical error calculations at a number of ten jackknife bins.

MGME simulations are designed to sample configurations with M values in-between $M_-=0$ and $M_+=m_0V$ with finite and large probabilities. Some probability distribution functions $P_{MGME}(M)$ from MGME2 simulations, for the occurrence of magnetization M values within Z_{MGME}, are displayed in Fig. 4. The top panel contains probabilities in 2D on 30^2 and 140^2 boxes, which were obtained with the run parameters in Table I, while the bottom panel shows 3D data on 16^3 and 40^3 boxes again with run parameters as in Table

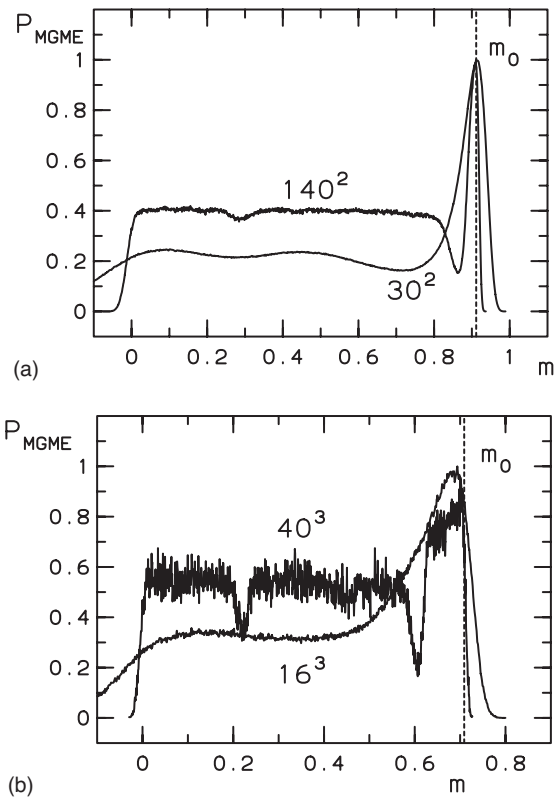

FIG. 4. (a) Multihistograms $P_{MGME}(m)$ in 2D from MGME2 simulations with the number of Gaussians as given in Table I. We display data with box volumes $L^2=30^2$ and 140^2. (b) Multihistograms $P_{MGME}(m)$ in 3D from MGME2 simulations with the number of Gaussians again as given in Table I. The box volumes are $L^3=16^3$ and 40^3. The vertical lines in both figures correspond to the Ising-models bulk magnetization value m_0. The maximum values of $P_{MGME}(m)$ were normalized to unity.

I. Phase space is covered with finite probabilities for magnetization density values that range from $m\approx 0$ up to densities somewhat larger than $m\approx m_0$. The distribution functions however, are not flat. They exhibit a marked surplus in the vicinity of the bulk-magnetization values, and at least two diplike depletion regions. For small m values the latter correspond to the droplets shape transitions from a slab to a circular droplet in 2D and from a slab to a cylinder in 3D [29]. The right-hand sided dips at large m values mark the evaporation-condensation (E/C) phase transition from a gas of small droplets to a single large nucleated droplet. The 3D shape transition from a sphere to a cylinder is not visible. The dip positions have large finite-size rounding corrections, as compared to their predicted values (see Refs. [5,22,29]). The canonical probabilities $P(M)$ as obtained from these data are displayed in Fig. 1.

Our final results for Binder's interface tension σ_B [Eq. (2.5)] from the MGME2 simulations in the 3D Ising model are given in Table II. The infinite volume extrapolation of σ_B used an identical approach as described in Ref. [22]. The MGME2 data are compared to a multicanonical ensemble simulation at otherwise identical parameter values. In particular, the number of local spin updates in the MGME2 simulation is the same as the one in the multicanonical ensemble simulation. Within error bars we find compatible results and, comparing the size of statistical error bars, both algorithms are of similar performance.

For the 2D Ising model we directly compare MGME1 and MGME2 simulations with flat-histogram multicanonical ensemble simulations (muca) [2,3], and with Wang-Landau (WL) simulations [7,8], all for the sampling of the probability $P(M)$ and the determination of σ_B. For purposes of a fair comparison, the total number of local Monte Carlo steps in each of the four approaches is kept the same. This means, e.g., that on the 140^2 lattice a total of 71×10^6 sweeps is simulated in the multicanonical ensemble. In particular, multicanonical ensemble simulations with a flat histogram (muca) use the multicanonical weight

$$e^{W_{muca}(M)} = \text{const}\, e^{-\ln P(M)}, \tag{4.4}$$

where $P(M)$ is the magnetization probability distribution function as obtained from previous MGME1 or MGME2 simulations. Finally, Wang-Landau simulations have originally been introduced to sample the energy density of states, but can easily be modified to magnetic systems for the sampling of the probability $P(M)$. Let us note that Wang-Landau simulations depend on a parameter value $f=\exp(\epsilon)\approx 1+\epsilon$,

TABLE II. Finite-size results for Binder's interface tension σ_B [Eq. (2.5)] from MGME2 Ising-model simulations in 3D at $\beta=0.2439$ in the third column. L denotes the box size. The second column contains data from a flat-histogram multicanonical ensemble simulation at an identical number of local Monte Carlo steps [22]. $\overline{\sigma_B}$ denotes the mean and columns five and six display deviations from the mean in units of the mean statistical error for the corresponding data sets. The last row contains infinite volume extrapolated results.

L	σ_B (Ref. [22])	σ_B, MGME2	$\overline{\sigma_B}$	$[\sigma_B-\overline{\sigma_B}]/\delta\overline{\sigma_B}$	$[\sigma_B-\overline{\sigma_B}]/\delta\overline{\sigma_B}$
16	0.069 89(13)	0.070 07(11)	0.069 99(09)	0.94	−1.21
20	0.072 54(13)	0.072 61(07)	0.072 60(06)	0.28	−0.88
24	0.073 49(11)	0.073 49(20)	0.073 49(10)	−0.04	0.01
28	0.073 63(14)	0.073 53(13)	0.073 58(09)	−0.47	0.58
32	0.073 67(13)	0.073 87(16)	0.073 75(10)	1.22	−0.75
36		0.073 56(21)	0.073 56(21)		
40		0.073 60(13)	0.073 60(13)		
∞	0.074 03(30)	0.073 76(25)	0.073 87(19)	−0.57	0.84

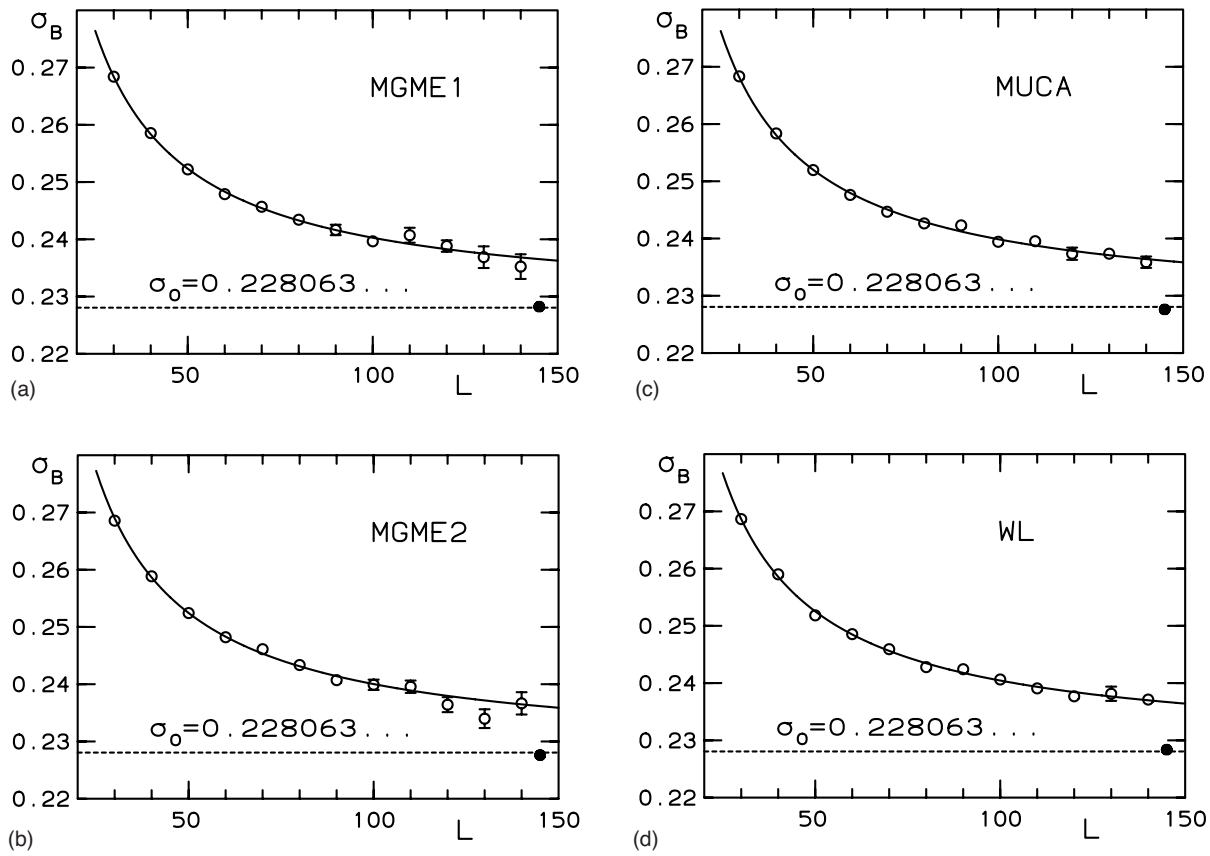

FIG. 5. From top to bottom and from left to right: (a) 2D results for Binder's interface tension [Eq. (2.5)] at $\beta=0.5$ in the Ising model from MGME1 simulations, (b) from MGME2 simulations, (c) from flat-histogram multicanonical ensemble muca simulations, and (d) from WL simulations. The dashed horizontal lines mark the infinite-volume exact result $\sigma_0=0.228\,063\ldots$. The solid circles in all panels denote the infinite-volume extrapolations using the fit Eq. (4.5). The fit results can be inspected in Table III.

which together with $g(E)$ is tuned towards a final value $f_{\text{final}}\approx 1$ very close to unity. Within their scheme f, or for that matter ϵ, is used to update the density of states with probability unity $\ln g(E)\to\ln g(E)+\epsilon$ at energy E for each local Monte Carlo step. A similar update exists for the magnetic case: $\ln P(M)\to\ln P(M)+\epsilon$ at magnetization M. The data presented in this paper stem from simulations with $\epsilon_{\text{final}}=0.000\,01$ or $f_{\text{final}}=1.000\,010$. Again $P(M)$ from previous MGME1 or MGME2 simulations is used as an input to Wang-Landau simulations and thus the somewhat delicate tuning of f, generic to Wang-Landau simulations, is avoided. We start directly with simulations at $f=f_{\text{final}}$ and from an already quite precise probability $P(M)$.

The lattice-size L dependence of Binder's magnetic interface tensions [Eq. (2.5)] and fits to the data with the form Eq. (4.5) for all of our simulations in the 2D Ising model, are displayed in the four panels of Fig. 5. The finite-size dependence of these data is extremely well reproduced by

$$\sigma_B(L)=\sigma_B+\frac{a}{L} \tag{4.5}$$

and the simple matching of the fit parameters, as well as the magnitude of fit parameter errorbars, demonstrates that all Monte Carlo methods compete on the same level of accuracy and computational efficiency. The fit parameters are found in Table IV and correspond to fits including all data points. The capillary droplet model in 2D predicts the presence of $1/L$ and the absence of $\ln(L)/L$ finite-size corrections for Binder's interface estimate in full accordance with our findings. If we compare the finite-size behavior of Binder's magnetic interface tension with Onsager's exact result for the antiferromagnetic seam, as given in Ref. [30], we find that the $1/L$ correction of Eq. (4.5) is not present in Onsager's result, where the asymptotic approach to the value σ_0 is actually from below. This can be explained by the different setup of both calculations. Onsager's calculation contains a single-line defect of length L in a system of size L^2 with periodic boundary conditions, while our simulation for Binder's definition in the same system of size L^2 contains two independently fluctuating domain walls of length L which interact via entropic repulsion. This effect gives a positive contribution to the free energy that explains the deviation from Onsager's result for finite L.

Finally, we display in Fig. 6 the statistical errors $\delta\sigma_B$ on finite-sized σ_B data as a function of the lattice size L. The three panels compare the statistical errors of MGME2 simulations (circles connected with solid polygons) with the errors of MGME1 (panel a), WL (panel b), and muca (panel c) simulations. Error bars are gently rising with increasing system size (at the given statistics), but none of the different approaches wins the competition with large error-bar reduc-

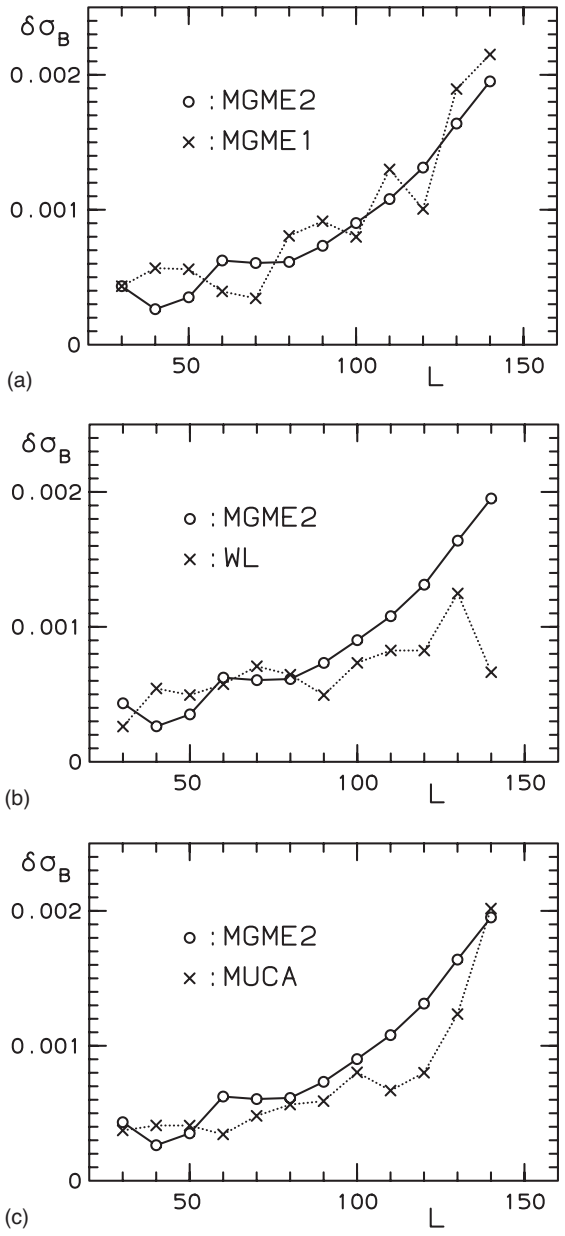

FIG. 6. The statistical errors $\delta\sigma_B$ on finite-sized σ_B data as a function of the lattice size L comparing MGME2 simulations with MGME1 (a), WL (b), and muca (c) bab simulations.

tion factors. Wang-Landau simulations are possibly better by a factor of 2 in error bars (factor of 4 in efficiency) on a large system, but again one has to take into account the effort of f tuning for Wang-Landau simulations, and that one will most likely level off a performance gain.

V. CONCLUSION

Within the present work, MGME simulations for the Monte Carlo sampling of such interesting things like barrier-free energies or density of states are introduced. MGME simulations populate phase through the superposition of probabilities from a multitude of single GMEs, and using parallel tempering, ergodicity is restored to a degree of efficiency, which for the considered case was similar to multicanonical ensemble simulations. Unlike in multicanonical ensemble simulations, there is, however, no weight factor on the input side of the simulation, and once the number N of GMEs is chosen to be large enough, the benefits of MGME simulations are expected to become apparent. And, unlike in Wang-Landau simulations, no particular parameter tuning towards $f_{\text{final}} \approx 1+\epsilon_{\text{final}}$ is needed. For any step on the Markov chain of MGME simulations an N-tuple of configurations has to be kept in the memory of a computer, and thus some price has to be paid. On the other hand, MGME simulations are predestined to be implemented on parallel computers and memory limitations there are far less serious than on single-node machines. A somewhat related approach of Laio and Parrinello [31] also employs Gaussian bias potentials in an attempt to cover free-energy landscapes. Their "metadynamics" simulations, however, just like Wang-Landau simulations at finite step size ϵ, are out of equilibrium, and thus a final map into a Markovian process is considered [32].

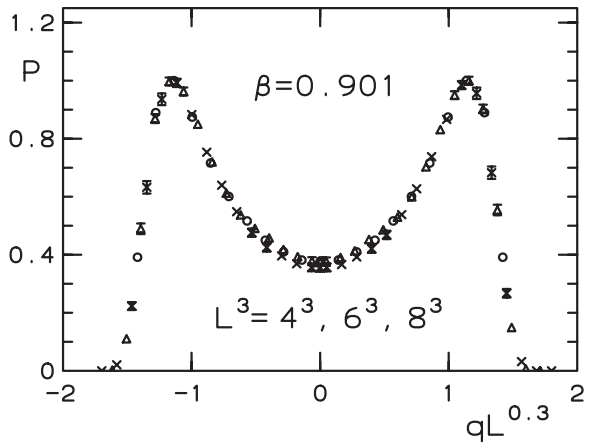

FIG. 7. Parisi overlap order-parameter density $q=Q/V$ distribution P as a function of the scaled $qL^{0.3}$ in the 3D EA spin-glass model. Lattice sizes are 4^3 (circles), 6^3 (triangles), and 8^3 (crosses). The inverse temperature is $\beta=0.901$, close to criticality, and the data can be directly compared to a figure in Kawashima's and Young's work [34].

One of the main concerns for Monte Carlo sampling methods of free-energy landscapes is the scalability to large system sizes and/or the scalability to large free-energy barrier values. The issue has two aspects: one is the effective performance of some algorithm for the solution of a particular problem; the other is the principal behavior in some asymptotic region of the parameters, like the lattice size L or the temperature. In the present work, we show for a particular simple and well understood problem that the efficiency of all three competitors, muca, MGME, and Wang-Landau simulations, is in fact quite similar. In particular, we tuned the number N of GMEs within MGME simulations linear with the 2D or 3D barrier size, and that is enough to determine barriers precisely, efficiently, and competitively. We emphasize that MGME simulations are free of recursive or iterative elements. Even an equal-spaced partition of Gaussians performs at the level of muca and WL simulations once $N \approx F_B$.

The case of a rough free-energy landscape has already been studied in an exploratory work. Using an N tuning of the kind $N \propto L^2$ in 3D, we display in Fig. 7, for purposes of illustration, the fixed-point shape of the Parisi overlap order-parameter [33] density $q=Q/V$ distribution, at a value of the inverse temperature $\beta=0.901$, close to criticality, on 4^3, 6^3, and 8^3 lattices for the Edwards Anderson spin-glass model. The average over frustrations for each lattice contains a sum over several thousand realizations, which was mastered with MGME simulations without ever fine tuning anything. Neither the multicanonical weight factors, nor the f tuning of Wang-Landau simulations, had to be babied on the set of all frustrations in any way.

The asymptotic performance of free-energy barrier Monte Carlo sampling is a nontrivial issue, as was recently demonstrated for multicanonical ensemble simulations of mixed phases in 2D: The hidden free-energy barrier at the so-called crystal-shape phase transition yields some residual exponential slowing down [5]. One must expect that all competitors, muca, MGME, and Wang-Landau simulations are affected by such free-energy singularities, but the situation remains far from being clear today, especially for the case of rough free-energy landscapes and mixed phases in higher-dimensional systems.

Finally, we note that recently some work went into improvements of multicanonical ensemble simulations via non-flat histogram sampling [35] and also into the feedback improvement of parallel tempering [36,37]. It would be interesting to apply these ideas to the current problem.

ACKNOWLEDGMENTS

T.N. thanks K. Rummukainen and Ph. de Forcrand for the discussions that initiated the project. The simulations were carried out with a number of privately owned Pentium Pc's, two dual Xeon workstations at the University of Bielefeld, and with an Opteron cluster at the NIC Jülich. T.N. also acknowledges the kind hospitality of the CBB group at the NIC in Jülich.

[1] G. M. Torrie and J. P. Valleau, J. Comput. Phys. **23**, 187 (1977).
[2] B. A. Berg and T. Neuhaus, Phys. Lett. B **267**, 249 (1991).
[3] B. A. Berg and T. Neuhaus, Phys. Rev. Lett. **68**, 9 (1992).
[4] A. M. Ferrenberg and R. H. Swendsen, Phys. Rev. Lett. **63**, 1195 (1989).
[5] T. Neuhaus and J. S. Hager, J. Stat. Phys. **113**, 47 (2003).
[6] B. A. Berg, Fields Inst. Commun. **26**, 1 (2000).
[7] F. Wang and D. P. Landau, Phys. Rev. Lett. **86**, 2050 (2001).
[8] F. Wang and D. P. Landau, Phys. Rev. E **64**, 056101 (2001).
[9] J. H. Hetherington, J. Low Temp. Phys. **66**, 145 (1987).
[10] M. S. S. Challa and J. H. Hetherington, Phys. Rev. Lett. **60**, 77 (1988).
[11] M. S. S. Challa and J. H. Hetherington, Phys. Rev. A **38**, 6324 (1988).
[12] D. P. Landau (private communication).
[13] G. Bhanot, R. Salvador, S. Black, P. Carter, and R. Toral, Phys. Rev. Lett. **59**, 803 (1987).
[14] P. Virnau and M. Müller, J. Chem. Phys. **120**, 10925 (2004).
[15] C. G. Geyer, in *Computing Science and Statistics*, Proceedings of the 23rd Symposium on the Interface, edited by E. M. Keramidas (Interface Foundation, Fairfax, 1991), pp. 156–163.
[16] A. P. Lyubartsev, A. A. Martsinovski, S. V. Shevkanov, and P. N. Vorontsov-Velyaminov, J. Chem. Phys. **96**, 1776 (1992).
[17] E. Marinari and G. Parisi, Europhys. Lett. **19**, 451 (1992).
[18] K. Hukusima and K. Nemoto, J. Phys. Soc. Jpn. **65**, 1604 (1996).
[19] M. E. Fisher, J. Stat. Phys. **26**, 87 (1969); V. Privman and M. E. Fisher, J. Stat. Phys. **33**, 385 (1983).
[20] S. Klessinger and G. Münster, Nucl. Phys. B **386**, 701 (1992).
[21] M. Hasenbusch and K. Pinn, Physica A **245**, 366 (1997).
[22] B. A. Berg, U. Hansmann, and T. Neuhaus, Z. Phys. B: Condens. Matter **90**, 229 (1993).
[23] L. Onsager, Phys. Rev. **65**, 117 (1944).
[24] P. A. Rikvold, H. Tomita, S. Miyashita, and S. W. Sides, Phys. Rev. E **49**, 5080 (1994).
[25] L. G. MacDowell, P. Virnau, M. Müller, and K. Binder, J. Chem. Phys. **120**, 5293 (2004).
[26] M. Pleimling and W. Selke, J. Phys. A **33**, L199 (2000).
[27] M. Biskup, L. Chayes, and R. Kotecky, Europhys. Lett. **60**, 21 (2002).
[28] A. Nussbäumer, E. Bittner, and W. Janke, in *Proceeedings of "Lattice 2005 International Symposium on Lattice Field Theory"*, PoS (LAT 2005), p. 252.
[29] G. D. Moore, K. Rummukainen, and A. Tranberg, J. High Energy Phys. 0104, 17 (2001).
[30] P. G. Watson, in *Phase Transitions and Critical Phenomena*, edited by C. Domb and J. L. Lebowitz (Academic Press, London, 1972), Vol. 2.
[31] A. Laio and M. Parrinello, Proc. Natl. Acad. Sci. U.S.A. **99**, 12562 (2002).
[32] G. Bussi, A. Laio, and M. Parrinello, Phys. Rev. Lett. **96**, 090601 (2006).
[33] G. Parisi, Phys. Rev. Lett. **50**, 1946 (1983).
[34] N. Kawashima and A. P. Young, Phys. Rev. B **53**, R484 (1996).
[35] S. Trebst, D. A. Huse, and M. Troyer, Phys. Rev. E **70**, 046701 (2004).
[36] H. G. Katzgraber, S. Trebst, D. A. Huse, and M. Troyer, J. Stat. Mech.: Theory Exp. 3, 18 (2006).
[37] S. Trebst, M. Troyer, and U. H. E. Hansmann, J. Chem. Phys. **124**, 174903 (2006).